

Advanced materials for family of fuel cells: a review of polymer electrolyte membrane

Thu Thi Pham¹, Majid Monajjemi^{1,2,*} , Fatemeh Mollaamin¹ , Chien Mau Dang^{1,*} ¹Institute for Nanotechnology (INT)- Vietnam National University, Vietnam²Department of chemical engineering, Central Tehran Branch, Islamic Azad University, Tehran, Iran*corresponding author e-mail address: dmchien@yahoo.com; maj.monajjemi@iauctb.ac.ir | Scopus ID : [54406655100](https://scopus.com/authid/detail.url?authorID=54406655100); [6701810683](https://scopus.com/authid/detail.url?authorID=6701810683)

ABSTRACT

Hydrogen is an important energy carrier and a strong candidate for energy storage. It will be a useful tool for storing intermittent energy sources such as sun. Hydrogen is a versatile energy carrier that can be used to power nearly every end-use energy need. By this work, modeling and controlling of ion transport rate efficiency in proton exchange membrane (PEMFC), alkaline (AFC), direct methanol (DMFC), phosphoric acid (PAFC), direct forming acid (DFAFC), direct carbon fuel cell (DCFC) and molten carbonate fuel cells (MCFC) have been investigated and compared together. Thermodynamic equations have been investigated for those fuel cells in viewpoint of voltage output data. Effects of operating data including temperature (T), pressure (P), proton exchange membrane water content (λ), and proton exchange membrane thickness (d_{mem}) on the optimal performance of the irreversible fuel cells have been studied. Performance of fuel cells was analyzed via simulating polarization and power curves for a fuel cell operating at various conditions with current densities. SOFC (Solid oxide fuel cell) is usually combined with a dense electrolyte sandwiched via porous cathode and anode and SORFC (Solid oxide regenerative fuel cell) is a subgroup of RFC with solid oxide regenerative fuel cell. SORFC operates at high temperature with high efficiency and it is a suitable system for high temperature electrolysis.

Keywords: Fuel cells, PEMFC, DFAFC, DCFC, polymer electrolyte.

1. INTRODUCTION

Fuel cells, already used widely throughout the economy, offer; 1 - small power units in the ranges between hundreds of watts to milli-watts, providing energies for extended operating systems, such as portable computers, vehicle's devices, video, cameras, mobile equipment, and or in industrial applications such as signaling and controlling devices. 2- Higher efficiency in the utilization of natural fuels. 3- A proportional decrease in the exhaust of combustion products. 4 - Improving operation of power level through loading and leveling with large-scale systems for temporary powering storage. 5 - A widely developed level of decentralized, silent, local power supply or as a combined power. 6 - Using an emergency power supply and control systems in individual installations such as research centers and hospitals. 7- Traction power around tens of kilowatts for large-scale application for electric cars, leading to cleaning the ecological situation in grand cities and populated area. 8- Power supplying to spacecraft, submarines, offshore and other underwater structures for supplying drinking water. Based on these reasons, the investigation of fuel cells has been considered by the end of 2019. By the end of the twentieth century, interest in fuel cells appears more common and global due to the dwindling world resources of oil and more serious ecological matters in big cities were recognized. Today, numerous and various fuel cells have been operated successfully, on a scale among tens of megawatts and tens or hundreds of kilowatts. Fuel cells are already making a high percentage contribution for solving economic and ecological matters facing mankind that without any doubt this contribution will continue to increase time by time. Recently, R&D attempts concerning the investigating, developing and application of fuel cells are guided in many countries, in national laboratories, in science research centers, universities, and in industrial portions [1-4]. Fuel cells are categorized based on species of their electrolytes and also by the difference in startup time ranging between around

one second for PEMFC [4] to ten minutes for solid oxide fuel cells (SOFC) with maximum efficiency between, 45% up to 60%. In the fuel cell of a solid acid electrolyte, H⁺ conducting oxyanion salt (solid acid) consists of a solid supported within the membrane which is saturated with H₂O for any further ions transporting. Anode reaction is: $H_2 \rightarrow 2H^+ + 2e^-$ and Cathode reaction is: $1/2 O_2 + 2e^- + 2H^+ \rightarrow H_2O$ and the overall reaction is: $H_2 + 1/2 O_2 \rightarrow H_2O$.

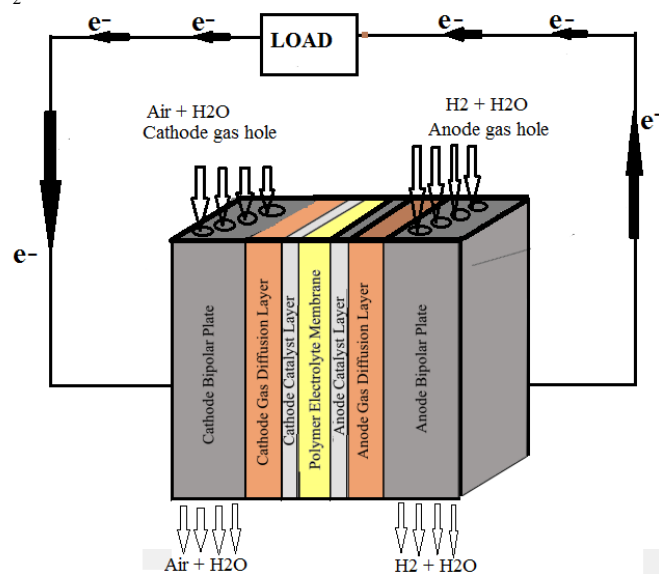


Figure 1. One unit of PEM fuel cell structure.

In viewpoint of mechanism, at the anode, H₂ first comes into contact with a nickel catalyst and breaks apart, bonding to the nickel surface forming weak H-Ni bonds consequently the oxidation reaction can proceed (Fig.1). Each H₂ releases its electron which moves around the external circuit to the cathode which is the electrical current. Then, the H⁺ bonds with H₂O on the membrane surface for forming H₃O⁺ that move through the

membrane to the cathode electrode, leaving the nickel catalyst for the next H₂. At the cathode, O₂ comes into contact with a nickel catalyst on the electrode surface and break apart bonding to the nickel sheet forming weak O-Ni bonds, enabling the reduction reaction to proceed. O₂ then leaves the nickel catalyst site, combining with two electrons that move in external circuit and two protons that have moved through the membrane for forming H₂O. Increasing the H₂ storage is a major section for the transition of more and more hydrogen molecules in a fuel cell [4, 5]. Direct methanol fuel cell (DMFC) is a subcategory of PEMFC in which methanol is used as the fuel (Fig.2). The advantages which can be considered are the energy-dense, easiness of transport and reasonably stable liquid at all environmental situations and meanwhile its disadvantages are low efficiency(around 10%), so they are targeted especially to portable applications, which power densities are more important than the efficiencies[6].

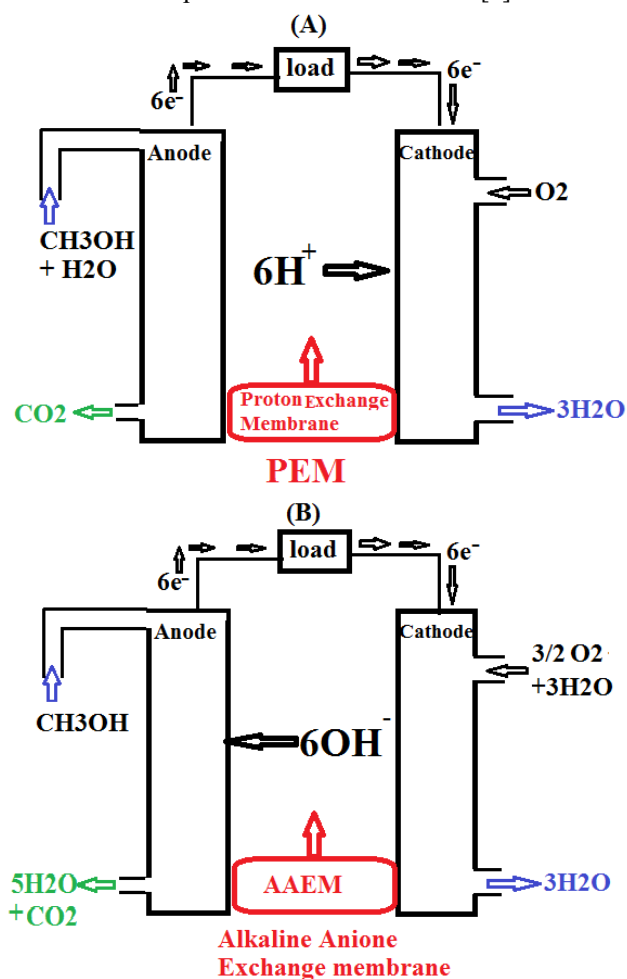


Figure 2. Direct methanol fuel cell (DMFC) with two kind electrolytes A: PEM and B: AAEM.

In contrast to indirect fuel cells, which CH₃OH molecules are reacted to H₂ molecules via a steam improving, direct form use a CH₃OH solution for transporting the reactant into the cells; common operating temperature is in the range 55–115 °C, which high temperature is generally pressurized [6,7]. Direct methanol fuel cell, itself is more efficient at top temperature and pressure, but these situations finally creating so many problems in the whole of the system that the advantage windswept, so atmospheric-pressure forms are yet preferred and applied [7, 8]. Due to the CH₃OH "cross-over" phenomena or diffusion via the membrane (without reacting), CH₃OH is unsuitable as a solvent that

decreases the performance of fuel cells considerably, since this phenomenon, directly reacts with air (in cathode), consequently reduction of the cell voltage accomplishes, therefore "cross-over" phenomenon is the main problem in inefficiency of direct methanol fuel cells [9]. This matter can be reduced through improving membranes, developing catalyst layers, reclaiming the structure of gas layers and optimizing the design of the electrodes (such as management of carbon dioxide at the anode) in viewpoint of current densities distribution [10]. The DMFC has restricted the PT factor (power*time) which means they can produce a small quantity of power in a lengthy period of time. Of course, those are suitable for large vehicles. The half-reactions of DMFC are an anode (oxidation): $CH_3OH + H_2O \rightarrow 6H^+ + 6e^- + CO_2$ and in cathode (reduction) the half-reaction: $\frac{3}{2}O_2 + 6H^+ + 6e^- \rightarrow 3H_2O$ while the overall reaction is: $CH_3OH + \frac{3}{2}O_2 \rightarrow 2H_2O + CO_2$ (Fig.2a).

The CH₃OH oxidation over the catalyst layers produces CO₂ and H₂O is consumed at the anode and is again produced at the cathode [9, 10]. From each reaction, 6-proton is transported through the PEM which usually is made of Nafion [2, 7] (sulfonate tetra-fluoro-ethylene based fluoro copolymer. Although Pt as a Nanoparticle might be a suitable catalyst for both anode and cathode, it is very expensive and during oxidation, the number of available sites in Pt will be occupied by CO which is produced in oxidation of methanol, consequently the efficiency of the cell will decrease. An alloy of platinum with a suitable percentage of Au, Ru and Cu can remove this problem. Storage of formic acid materials (HCOOH) is secure, safe, and confident compared to H₂, as it is a non-flammable liquid and also does not cross over the polymer membrane, so its performance can be higher than that of methanol. DFAFC converts HCOOH and O₂ into CO₂ and H₂O to produce energy. The half-reactions of DFAFC are anode: $HCOOH \rightarrow CO_2 + 2H^+ + 2e^-$ and in cathode: $\frac{1}{2}O_2 + 2H^+ + 2e^- \rightarrow H_2O$ and total reaction is $HCOOH + \frac{1}{2}O_2 \rightarrow CO_2 + H_2O$ [11]. The alkaline fuel cell (Bacon) is one of the most important fuel cells with high performance that NASA has applied (Fig.2b), in Apollo-series missions and on the space shuttles. The half-reactions of DFAFC are anode: $H_2 + 2OH^- \rightarrow 2H_2O + 2e^-$. And in cathode: $O_2 + 2H_2O + 4e^- \rightarrow 4OH^-$. In AFC, two electrodes are divided through a porous materials filled with an alkaline solvent, such as KOH, NaOH or NH₄OH. One of the important advantages of these kinds fuel cells is that alkaline solutions can react with CO₂ to produce conversion K₂CO₃. Environmentally, AFC is suitable to clean out as much of the CO₂ due to operating (even in high temperature) on pure oxygen, or at least purified air. Since O₂ reduction reaction (ORR) at the cathode is easier than in acidic cells, AFCs in the systems can be operated up to 90 °C with higher performance than acidic electrolyte, such as PEMFC.

RFC (regenerative or reverse fuel cell) is a fuel cell run in reversible situation, that uses electricity and chemical molecules(1) to chemical molecules (2). The main item is that the process of fuel cell must be reversible. Although a given system is usually minimized for operating in one step, it may not be built in such a way that it can be operated backwards. The mechanism of the reverse fuel cell is based on H₂ fueled proton exchange

membrane fuel cell. As for instance, it is used H_2 and O_2 to produce electricity with H_2O ; a regenerative hydrogen fuel cell is used electricity and water for producing H_2 and O_2 . During the operating in reverse step, the anode for the electricity level becomes the cathode in the H_2 generation, which means reverse fuel cell mode, and vice versa. When an external voltage is used, H_2O at the cathode side will undergo electrolysis to produce H^+ and O^{2-} ions; O^{2-} will be transported via the electrolyte towards anode where it can be oxidized to form O_2 . In this reverse level, the polarity of the cell is opposite to that for the fuel cell. At cathode: $H_2O + 2e^- \rightarrow H_2 + O^{2-}$ At anode: $O^{2-} \rightarrow 1/2O_2 + 2e^-$ Overall: $H_2O \rightarrow 1/2O_2 + H_2$ (Fig.3).

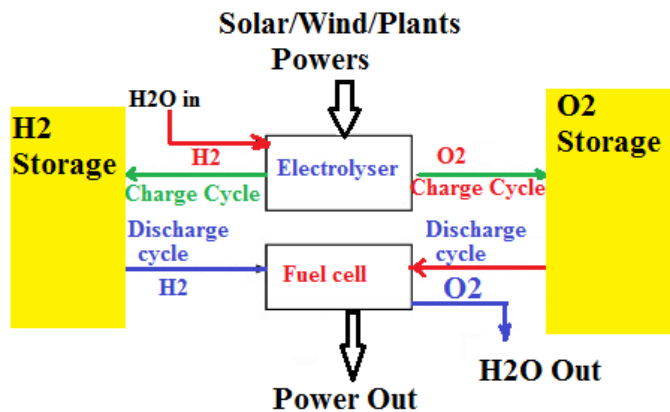


Figure 3. A schematic of regenerative fuel cell.

SOFC (Solid oxide fuel cell) is usually combined with a dense electrolyte sandwiched via porous cathode and anode as shown in Fig. 3. The fundamental power densities of SOFCs are around $500\text{--}600\text{ mW cm}^{-2}$ at 0.75 V , corresponding to an area-specific resistance (ASR) value of $0.40\text{ }\Omega\text{cm}^2$ for the whole cell via assuming the open circuit voltage (OCV) of around 1 V . Although the most power densities might ideally reach to 1000 mW cm^{-2} , this goal is difficult to be achieved at temperatures lower than $600\text{ }\Omega\text{cm}^2$. For increasing the activity of each section, different techniques might be applied based on the characteristics of the components. For a simple model, the ASR constitutes the polarization and the ohmic resistance of the complete fuel cell. The ohmic losses can be attributed mainly to the electrolyte resistances whereas the polarization losses are coming from both electrodes. The polarization losses should be further divided into the electrochemical, gas diffusion, and gas conversion losses. In both of them, the polarization losses need to be estimated, while in the anode, there are further polarization losses due to both diffusion and conversion. The ohmic electrolyte resistance might be determined through the $R_{o,E} = \frac{L_E}{\sigma A}$ where, $R_{o,E}$ is an ohmic resistance, σ is electrolyte ion conductivity, L_E is the thickness of the electrolyte, and A is the active area. For decreasing the ohmic resistance, one certain strategy is to fabricate thin film electrolytes, around 100 nanometers. In addition, novel electrolytes can be investigated. Obviously, finding new materials including enough high ionic conductivities and stabilities in highly reducing and oxidizing conditions over $510\text{ }^\circ\text{C}$ are not trivial and therefore, only a few materials have been used, such as YSZ-Ni cermet which is an important and popular anode for SOFCs [12]. The transmission-line approach can be applied for determining the electrochemical polarization resistance of these composite

anodes: $R_{P,A} = \sqrt{\frac{R^{LS}}{\sigma_{ion}L_{TPB}}} \coth(L_A \sqrt{\frac{L_{TPB}}{\sigma_{ion}R^{LS}}})$ (1) where, $R_{P,A}$ and R^{LS} are the anode resistance and the polarization resistance per unit length of a TPB line respectively, L_A is the anode thickness and L_{TPB} is the TPB length per unit electrode volume, and σ_{ion} is the effective ionic conductivities of the oxide phase. From this equation via increasing, L_{TPB} , $R_{P,A}$ will be decreased and the amount of L_{TPB} basically depends on the electrode morphology. In addition Nanoparticles adornment is an excellent way for increasing the L_{TPB} . MIEC or (Mixed ionic and electronic conducting compounds) are formally the best low-temperature cathode's materials given their huge oxygen surfaces exchange coefficients "k" and oxygen bulk diffusion coefficients " D_v ". For a thicker cathode than a characteristic depth l_δ for ion diffusion by a Nanoparticle size (less than l_δ), the Adler-Lane-Steele model [13] exhibits the effect of oxygen transport coefficients to the "chemical" resistance R_{chem} , as a factor to the cathode polarization resistance $R_{P,C}$, for MIEC electrode (a porous single phase) [14]: $R_{cheme} = \frac{RT}{4F^2} \frac{1}{\sqrt{4a \frac{(1-\varepsilon)}{\tau_{solid}} R_0 C_0 x_v^0 D_v}}$ (2) where F and R is

the Faraday and gas constants, C_0 is the concentration of mobile oxygen in the oxide, x_v^0 is the interstitial mole fraction of oxygen, τ_{solid} is the solid-phase tortuosity, ε and a are the fractional porosity and surface area to volume ratio, respectively. Meanwhile R_0 indicates the molar surface exchange rate which depends on the surface exchange coefficient via the mechanism of O-incorporation, and therefore depends also on the oxygen partial pressure p_{O_2} and O-ion defect concentration x_v^0 [15]. High oxygen vacancy concentration is needed for cathode materials due to oxygen bulk diffusion and surface exchange on the cathodes. Therefore they can be extracted via new doping strategies with advanced ion-transport channels. Such an effect is acceptable in viewpoint of the charge transfer rate in the electrodes via the particle size and the surface area of the catalyst. Since nanostructured electrode provides an enhanced electrode reaction rate, the polarization resistance of the electrode is effectively reduced at low temperatures. Formal powder processing, on the other hand, leads to microparticle sizes due to the micro raw powder sizes and coarsening during high-temperature sintering. Nano-approaches such as metal organic deposition, pulsed-laser deposition, spray pyrolysis, and sputtering, have accordingly been applied for any developing of nanostructured cathodes.

SORFC (Solid oxide regenerative fuel cell) is a subgroup of RFC with solid oxide regenerative fuel cell. SORFC operates at high temperatures with high efficiency and it is a suitable system for high temperature electrolysis. Less electricity is required for electrolysis process in SORFC due to high temperature. Although the electrolyte can be oxygen ion or hydrogen ion conducting, for oxygen ion conducting yttrium stabilized zirconia (YSZ) based SORFC using Ni-YSZ as the H_2 electrode and LSM-YSZ as the oxygen electrode has been investigated [16]. Dönitz and coworkers reported on the mechanism of YSZ electrolyte cell by the current density of 0.3 A cm^{-2} and 100% Faraday efficiency at only 1.05 V [17]. In one research, it has been exhibited that ceria-based composite electrolytes, where both proton and oxide ion conduction exist, produce high current output for fuel cell operation and high hydrogen output for electrolysis operation

[18]. A few doped atoms such as Zr with Sc and ceria (10ScCeSZ) are also investigated as potential electrolytes in SOFC for H₂ production at 550–750 °C. It is reported that 10ScCeSZ exhibits suitable properties with high current densities [19]. Generally used/tested electrodes are Ni/Zr cermet (Ni/YSZ) and La-substituted Sr and Ti composite for SOFC cathode, and La-Sr-Mn (LSM) for SOFC anode. Other anode materials can be La-Sr-Fe (LSF), La-Sr-Cu-Fe and La-Sr-Co-Fe (LSCoF). Studies exhibit that Ni/YSZ electrode was less active in reverse fuel cell operation than in fuel cell operation, and this can be attributed to a diffusion-limited process in the electrolysis direction, or its susceptibility to aging in a high-steam environment, primarily due to coarsening of nickel particles [20]. Therefore, alternative materials such as the Ti/ceria composite (La_{0.35}Sr_{0.65} TiO₃-Ce_{0.5} La_{0.5} O₂) or (La_{0.75}Sr_{0.25}) and (0.95Mn_{0.5}Cr_{0.5}O₃) (LSCM) have been proposed electrolysis cathodes. Both LSF and LSM/YSZ are reported as suitable anode candidates for electrolysis mode [21, 22]. DEFC (direct-ethanol fuel cell) is a system of fuel cell in which ethanol is fed directly into the cell. It has been used as a system to investigate a range of fuel cell mechanism including the use of PEM [23]. DEFC uses C₂H₅OH in the fuel cell instead of the more toxic CH₃OH. C₂H₅OH is a hydrogen-rich liquid and it has higher specific energy compared to CH₃OH. The use of C₂H₅OH would also overcome both the storage and infrastructure challenge of H₂ in fuel cell applications [24]. The DEFC, similar to the DMFC, relies upon the oxidation of ethanol on

a catalyst layer to form carbon dioxide. Water is consumed at the anode and is produced at the cathode.

Protons (H⁺) are transported across the proton exchange membrane to the cathode where they react with O₂ to produce water. Electrons are transported through an external circuit from anode to cathode, providing power to connected devices. Anode: C₂H₅OH + 3H₂O → 12H⁺ + 12e⁻ + 2CO₂, cathode: 3O₂ + 12 H⁺ + 12e⁻ → 6H₂O. SOFC (solid oxide fuel cell) is a system that produces electricity directly from oxidizing of a fuel consist of solid oxide. The most important advantage of this category equipment is a combination of heat and power efficiency, long-term stability, fuel flexibility, low emissions, and relatively low cost. The largest disadvantage is a high operating temperature

[25]. Generally, SOFC consist of four layers which three of them are ceramics and single cell consisting of these four layers stacked together is basically only a few millimeters thick. A few hundred of these unit cells are then connected in series for forming SOFC stack. The ceramics used in SOFC do not become active until they reach a very high temperature and as a result, the stacks have to run at temperatures ranging from 500 to 1,000 °C. Reduction of oxygen into oxygen ions occurs at the cathode. These ions can then diffuse through the solid oxide electrolyte to the anode where they can electrochemically oxidize the fuel. In this reaction, a water byproduct is given off as well as two electrons. These electrons then flow through an external circuit where they can do work. The cycle then repeats as those electrons enter the cathode material again [26].

2. MATERIALS AND METHODS

In 2005, several attempts have been applied for using fast oxygen ionic conductors as SOFC electrolytes instead of conventional YSZ such as doped-ceria, doped-lanthanum Gallate, and Scandia stabilized zirconia. A doped-ceria electrolyte, CERES has been fabricated in low-temperature for SOFCs which can be operated below 600°C. Basically, oxide-ion electrolyte is buildup of an oxygen-deficient fluorite or perovskite oxides that permits oxygen transport through oxygen vacancies. YSZ or Fluorite-structured zirconia-based electrolyte is important and general cathode material applied as the electrolyte in SOFCs given its high ionic conductivities and stabilities in oxidizing and reducing atmospheres. The ionic conductivities of YSZ between 600 and 800 °C are substantially lower than that of ceria-based electrolytes, Gadolinium-doped ceria (GDC) or lanthanum Gallate-based electrolytes, La_{0.8}Sr_{0.2}Ga_{0.8}Mg_{0.2}O₃, (LSGM). They are based on a criterion in which the electrolyte components might not contribute over than 0.15 Ωcm² to the total area specific cell's resistance; for the electrolyte with thickness of 16 μm, the associated specific Ionic conductivities can exceed 10–2 S cm⁻¹. In order for achieving this criterion; they should selected Gadolinium doped-ceria (GDC) of thickness between 12 to 35 μm. Due to low-cost methods for fabricating compressed GDC films on steel-supported structure, adopting a electrophoretic deposition (EPD) technique is needed. The layers of GDC10 (Ce_{0.9}Gd_{0.1}O_{0.95}, Rhoddia) were deposited on a steel substrate via EPD and accomplished through pressing with a Cold Isostatic Pressing machine. After sintering the pressed material at 950°C, thin and compressed films of GDC10 were fabricated successfully. With a LSGM electrolyte, Mitsubishi Materials Corp. in

collaboration with the Kansai Electric Power Company., Inc., has developed intermediate-temperature SOFCs. Cobalt-added LSGM by the formula of La_{0.8}Sr_{0.2}Ga_{0.8}Mg_{0.15}Co_{0.5}O_{3-δ} (LSGMC) were selected and fabricated through a conventional solid state reaction technique. The electrolyte has been designed with the adopted system below 850°C for the SOFCs using LSGMC around 190 μm thick electrolytes. In addition a calcined mixture of La₂O₃, SrCO₃, Ga₂O₃, MgO and CoO were mixed with organic binder; after disk-shape green sheets were fired at 1350 to 1550°C, 210 μm thick LSGMC electrolytes were obtained. In last decades, a seal-less planar-type SOFC module of 1 kW classes was constructed successfully using 25 cells in a diameter of 150 mm. Their operations were also successful in obtaining an outputting power of 1 kW without a heating system below 850°C.

2.1. Electrolytes and Novel Oxide-Ion Conductors.

The electrolyte for SOFC generally consists of a dense solid metal-oxide cermet such as zirconia (ZrO₂) with 10% yttrium added as a dopant, known as yttria-stabilized zirconia (YSZ); this mixture allows for good conduction of oxygen ions in the range of 600–950°C. Scandium-stabilized zirconia was also supposed, as it exhibits the highest ionic conductivities and sufficient stabilities both in oxidizing and reducing systems which lead to suitable long-term stabilities due to YSZ. Moreover, a number of ionic conductors have been investigated such as La_{1-x}Sr_x Ga_{1-y} Mg_y O_{3-(x+y)/2} (LSGM) & La₂Mo₂O₉ (LAMOX); Bi₄V_{2-x}M_xO_{11-y} (BIMEVOX). Various pyrochlores with relatively high ionic transport properties, such as (Gd, Ca)₂Ti₂O_{7-δ}; materials derived from Ln_{10-x}Si₆O_{26±δ}, where Ln represents a lanthanide-

series element. In addition, with the goals of reducing operating temperature, both proton-conducting materials and ceria-based electrolytes might be considered (Fig.4).

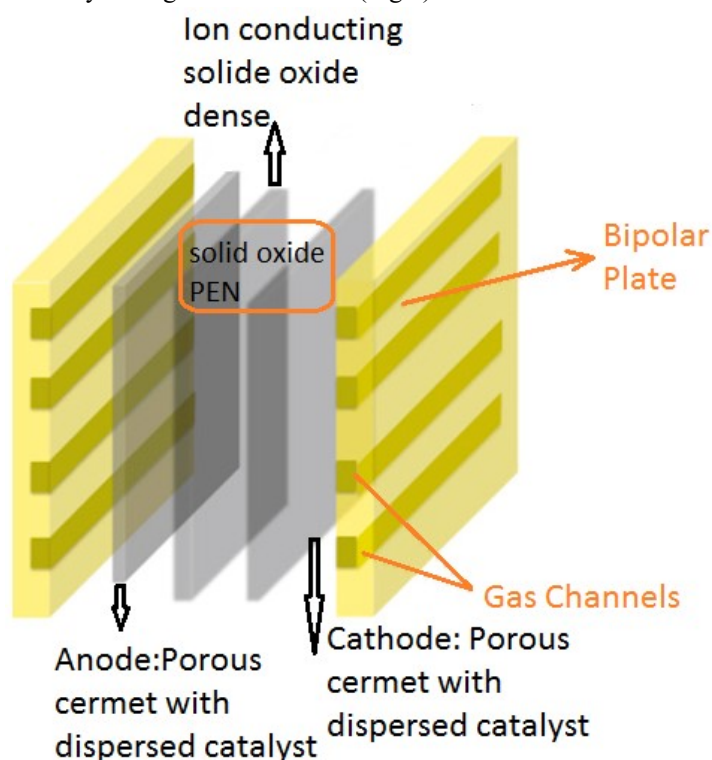


Figure 4. A schematic of solid oxide (PEN).

Usually, oxide-ion electrolytes consist of oxygen-deficient fluorite or a perovskite oxide which permits oxygen transporting through vacancies. As mentioned above, YSZ, are the most general materials applied as the electrolyte in SOFCs due to its high ionic conductivities and stability in oxidizing and reducing atmospheres. The ionic conductivity of YSZ at intermediate temperatures (between 600 and 900 °C) is substantially lower than that of ceria-based electrolytes, i.e., gadolinium-doped ceria (GDC) or lanthanum gallate-based electrolytes, i.e., $\text{La}_{0.8}\text{Sr}_{0.2}\text{Ga}_{0.8}\text{Mg}_{0.2}\text{O}_{3-\delta}$ (LSGM). ($\delta\text{-Bi}_2\text{O}_3$) in a fluorite structure has the highest oxygen ionic conductivities in SOFC electrolytes which are afforded through a combination of a high concentration of oxygen vacancies and high anion mobility [27-29]. Verkerk tested Dy_2O_3 doped Bi_2O_3 system and synthesized $\delta\text{-Bi}_2\text{O}_3$ (fcc) structure [30] and then Takahashi et al. investigated Gd_2O_3 doped Bi_2O_3 system and obtained fcc structure with Gd_2O_3 [31]. In both items, large dopant concentrations were applied for stabilizing the cubic structure. In the case of lanthanide dopant, the ionic radius and polarizabilities are linearly related. Although they can be stabilized the fcc bismuth oxide structure, the anion ordering rate is fastest for Yb and slowest for Dy due to large Polarizability of Dy^{3+} in comparison to Yb^{3+} . Co-doping causes the solid solubility range to depend on single dopant systems for cubic phase-stabilization, as for instance, high conductivities were observed from $(\text{DyO}_{1.5})_{0.08}(\text{WO}_3)_{0.04}-(\text{BiO}_{1.5})_{0.88}$ composition (8D4WSB). In the case of CeO_2 , n-type electronic conductivities are partially present at low oxygen partial pressures. Bi_2O_3 decomposes to metallic Bi with reducing systems; introducing similar operational issues. Jung & Wachsman [32] investigated a bilayer electrolyte consist of Er_2O_3 -stabilized Bi_2O_3 (ESB) on its cathode side and

GDC on its anode side. The blocking of the partial electronic conduction in CeO_2 by Bi_2O_3 layers enables close to theoretical OCV and a high power density (around 2000-2200 mW cm^{-2}) at 600 °C to be achieved for these kind bilayers

Electrodes of SOFCs; A few years ago, Goodenough suggested a structure of solid oxide-ion conductors family of $\text{Sr}_{1-x}\text{A}_x\text{Si}_{1-y}\text{Ge}_y\text{O}_{3-0.5(x+y)}$ ($\text{A} = \text{Na}$ and K). They characterized these materials' potential as an electrolyte for SOFCs [33]. Ionic conductive of $\text{Sr}_{1-x}\text{A}_x\text{Si}_{1-y}\text{Ge}_y\text{O}_{3-0.5(x+y)}$ is dependent on the strong tetrahedral site of Si^{4+} a layered (SrSiO_3)₃ structure instead of SrSiO_3 crystallization. Sr^{2+} in the (SrSiO_3)₃ forms close-packed planes with a trigonal-prismatic coordination divided through a layer of Si_3O_9 units. Si_3O_9 unit includes three $[\text{SiO}_4]$ tetrahedral where each $[\text{SiO}_4]$ tetrahedral sharing a corner in a triangular plane of oxygen atoms parallel to the Sr^{2+} sheets. The apical oxide ions on the $[\text{SiO}_4]$ tetrahedral is coordinated with Sr^{2+} and show direct close access to oxygen atom sites on neighboring Si_3O_9 complexes. $\text{Sr}_{0.8}\text{K}_{0.2}\text{Si}_{0.5}\text{Ge}_{0.5}\text{O}_{2.9}$ showed an oxygen conductivity of σ_0 around 10^{-2}cm^{-1} at 620 °C. This amount is comparable to the best oxide-ion conductor. When K^+ was replaced by a smaller electropositive such as Na^+ , the oxygen ionic conductivity is improved. Moreover, $\text{Sr}_{1-x}\text{Na}_x\text{SiO}_{3-0.5x}$ electrolytes are less hygroscopic than $\text{Sr}_{1-x}\text{K}_x\text{SiO}_{3-0.5x}$. SOFC based on $\text{Sr}_{0.55}\text{Na}_{0.45}\text{SiO}_{2.755}$ electrolyte were synthesized with an electrolyte by formula $\text{Sr}_{0.55}\text{Na}_{0.45}\text{SiO}_{2.755}$ which indicated maximum power densities with comparison to the best maximum power densities.

2.2. Protonic Conductors.

The efficiency of SOFC through oxide-ion electrolytes decreases the temperature and the high activation energy (E_a) for oxygen ion conduction. Since the activation energies for proton conduction are lower than the O^{2-} conduction, H-SOFCs might be acted among 200 and 500 °C. The simulated H-SOFCs efficiencies based on the existing properties of protonic ceramic fuel cell electrolyte is distributed between 250 and 1550 mWcm^{-2} at 300 to 650 °C, supposing a 10 micrometer thickness of electrolytes. Doped- BaCeO_3 and doped- BaZrO_3 have been investigated as proton conductors. Although there are large proton conductivities for the doped- BaCeO_3 , low chemical stabilities in H_2O and CO_2 appear practically. Doped- BaZrO_3 , on the other hand, exhibits high chemical stabilities. The highest proton conductivities for doped- BaZrO_3 were obtained through pulsed laser deposition (PLD) of $\text{BaZr}_{0.8}\text{Y}_{0.2}\text{O}_{3-\delta}$ (BZY20) onto oriented MgO substrate. Although via crystallinity and eliminating boundaries which block proton transport in the doped BaZrO_3 electrolyte, the proton conductivities of 0.01Scm^{-1} at 300 °C were shown an enhancing of stability for proton conducting electrolytes. Comparatively higher electronegative elements were doped for increasing the resistances toward the acidic CO_2 and to reduce the kinetics of BaCO_3 . Kannan fabricated $\text{Ba}_{0.5}\text{Sr}_{0.5}\text{Ce}_{0.6}\text{Zr}_{0.2}\text{Gd}_{0.1}\text{Y}_{0.1}\text{O}_{3-\delta}$ perovskite through substituting Ba with Sr and co-substituting Ce with Gd and Zr in Y-doped BaCeO_3 [34]. This doped perovskite showed high chemical stabilities when exposed to SOFC through-products of high proton conductivity. Despite its high stabilities against CO_2 and H_2O , $\text{BaCe}_{0.7}\text{Ta}_{0.1}\text{Y}_{0.2}\text{O}_{3-\delta}$ needs high sintering temperature. Through using In and Ta, $\text{BaCe}_{0.7}\text{Ta}_{0.1}\text{In}_{0.2}\text{O}_{3-\delta}$ merges the advantages of novel chemical stabilities and lower sintering temperature. Liu and coworkers fabricated $\text{BaZr}_{0.1}\text{Ce}_{0.7}\text{Y}_{0.2-x}\text{Yb}_x\text{O}_{3-\delta}$ (BZCYYb) mixed conductor, which features

simultaneously rapid oxide ion and proton transport [35]. ZCYb displayed large ionic conductivities at a relatively low temperature between 550–750 °C. The protons can significantly diffuse from the anode to the cathode parts with a chemical potential gradient. There is however no percolated pathway for the electrons. The electrons are thus forced to pass through the external circuit to generate electric power. The ionic conductivity of acceptor-doped materials is officially determined through the amount of O₂ vacancies.

2.3. Providing of Thin-Film Electrolytes.

For minimizing the ohmic resistance by decreasing temperature, the electrolytes need to be made thin, especially when the ionic conductivities of electrolyte materials are not high at mentioned temperatures. Several of methods for fabricating thin films have been used which the most widely are known as atomic layer deposition (ALD) [36], chemical vapor deposition CVD [37] and physical vapor deposition (PVD). Thin film electrolytes might be fabricated on porous supporting anode structures such as YSZ-NiO and SDC-NiO. In addition they can solve the mechanical strength and thermal problems if materials with high thermal stability and sufficient thicknesses in the supporting structure are used. Hong et al.[38] fabricated thin YSZ electrolytes via direct currents reactive magnetron sputtering process. Through controlling the Ar flow rate during the reactive sputtering, YSZ thin film featuring dense and suppressing columnar grains can be obtained. Using a low Argonne partial pressure of only 0.67 Pa during the deposition, a 235 nm-thick YSZ pinhole-free electrolyte was achieved. This cell produced maximum power densities of 158 mW cm⁻² at an OCV of 1.09 Volt under an argon flowing rate equal 20 sccm at 450 °C. LSGM conductivities are an order-of-magnitude higher than YSZ conductivity at 550 °C; making it a promising electrolyte for a SOFC operated below 650 °C. Various dual-layers electrolytes equal of 5 μm-thicks LSGM and 400 nm-thick SDCs were also made through PLD. The SDC buffer layers were deposited among the LSGM and the anode supporting. The optimal target compositions were determined to be La_{0.68}Sr_{0.19}Ga_{0.87}Mg_{0.27}O₃ while the optimal substrate temperature was 750 °C. These optimized LSGM thin films electrolyte based fuel cell provides Power density of 573 mili Watt cm⁻² at 500 °C. It is notable that the chemical solution deposition (CSD) process presents various superiorities inside vacuum deposition methods for thin-films

3. RESULTS

The details of the above fuel cells are summarized in table 1. The enthalpy of hydrogen combustion reaction or hydrogen heating amount for one mole of hydrogen can be calculated via $\Delta H = \Delta H_f^0(H_2O) - \Delta H_f^0(H_2) - \frac{1}{2}\Delta H_f^0(O_2) = -286.31 \text{ KJ/mol}$. Hydrogen heating amounts are used as a measure of energies input for the fuel cells and this is the maximum value of thermal energy which can be extracted from hydrogen. In addition Gibbs free energy is given by the following equation: $\Delta G = \Delta H - T\Delta S$. which the difference between entropies of products and reactants can be calculated as $\Delta S = \Delta S_f^0(H_2O) - \Delta S_f^0(H_2) - \frac{1}{2}\Delta S_f^0(O_2)$. The maximum electrical work is: $W_{max} = -n(emf)F = -\Delta G$ where F is Faraday’s constant and “emf” is the ideal electro motor force or potential of the cell. Therefore the

electrolyte low cost and scalability. YSZ nanoparticles were added into chemical solutions to counteract external constraints and minimize inhomogeneous densification. By reducing the sintering temperature, the electrolyte’s thickness can be further reduced. The structural stability of the substrate’s pores is determined by the overall thickness of the bilayer electrolyte, which enables the development of the bilayer electrolyte and optimum cell efficiency [39-55].

2.4. Modelling and simulation.

The details mechanism of the PEM fuel cells are very complex due to the different and tightly phenomenon which occur within a cell-fluid-dynamic, migration, electrochemical reaction, diffusions, water transports inside polymer membrane involving both electro-osmotic drag and back diffusion, proton transports via proton-conductivities of the polymer membranes, electron conduction via electrical conductivities of the cell components, heat transfer involving both conduction via solids components of the cells and convection of reactant gases and cooling medium, water transports both evaporation and liquids via porous catalyst layer and gas diffusion layer, and phase changes (scheme 4). Modelling and Processing and operating of a PEM fuel cel (Fig.5) is needed for describing the basica phenomenon to evaluate the cells steady-state and dynamic behavior. However, the complex mechanism inside the fuel cell causes challenging in some models involving reactants, cooling, and humidification and conditioning systems. Models are able to predict fuel cell efficiency under different operating situations and optimization and designing of control systems.

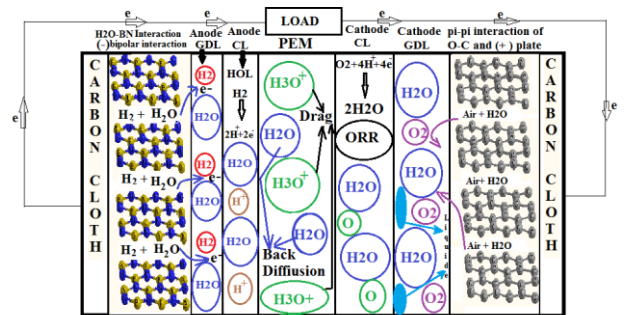


Figure 5. Processing and operating of a PEM fuel cell.

Based on our previous works this study has been simulated and investigated for any further discussion [56-86].

theoretical hydrogen/oxygen fuel cell potential or maximum voltage of fuel cells is: $emf = E = \frac{-\Delta G}{nF} = \frac{237.342 \text{ J mol}^{-1}}{2 \times 98486.5 \text{ Coulmb}} = 1.231 \text{ Volt}$. The thermal efficiency is defined based on the amount of useful energy released when a fuel is reacted with an oxidant (ΔG), relative to the change in stored chemical energy (ΔH) therefore the maximum theoretical yields in a fuel cell is $\eta = \frac{\Delta G}{\Delta H} = \frac{237.342}{-286.31} = \%82.9$. Based on Nernst equation a function of temperature and pressure can be applied for any fuel cells as; $emf = E_{(T,P)} = -\left(\frac{\Delta H}{nF} - \frac{T\Delta s}{nF}\right) + \frac{RT}{nF} \ln \left[\frac{P_{H_2} P_{O_2}^{0.5}}{P_{H_2O}}\right]$, (3). For both Phosphoric acid fuel cells (PAFC) and polymer electrolyte membrane fuel cells (PEMFC), the hydrogen molecules splitting

at the anode into hydrogen ions are transport across the electrolyte to the cathode. For a PEMFC of static electrolyte with 25 cm² active area, 50µm thickness and 9·10⁻⁷cm²·s⁻¹ diffusion coefficient of H⁺ ions, current density obtained for the applied potential difference between 0.5-1.0V at 75°C exhibited in Fig.6

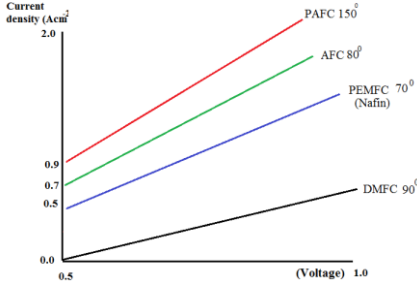


Figure 6. Current densities versus potential.

Although PEMFC has a lower current than PAFC, due to its lower operating temperature allowing fast startup and can be applied in automotive power applications. Another advantage of PEMFC is that its electrolyte is a solid material and is less expensive to manufacture than the liquid electrolyte $\eta(T, P) = \left(\frac{\Delta H - T\Delta S}{nF}\right) + RT \ln\left(\frac{P_{H_2} P_{O_2}^{0.5}}{P_{H_2O}}\right)$ (4). It is notable that, the maximum electrical energies and the potential differences are achieved when the fuel cells are operating under the thermodynamically reversible condition. Practically, an open circuit potential is considerably lower than the theory due to three main losses which are, first concentration polarization V_{concen} second activation polarization V_{act} , and third ohmic polarization V_{ohmic} . The irreversible voltage loss V_{irrev} is a summation of these three parameters, $V_{irrev} = V_{act} + V_{ohmic} + V_{concen}$. Based on Butler-Volmer equation, a specific potential is needed for overcoming to the energies barriers which called activation polarization $i = I_c + I_A = i_0 \left[-\exp\left(-\frac{\alpha_c n F \eta}{RT}\right) + \exp\left(\frac{\alpha_a n F \eta}{RT}\right) \right]$ (5) where I_A and I_c are anode and cathode current densities, respectively and i_0 is the reaction exchange currents densities. Meanwhile α_A and α_C are the charge transfer coefficients at the anode and cathode and n is the number of exchange protons per mole of reactant. Here η is the activation over potential term or $\Delta V_{act} = \eta = -\frac{RT}{n\alpha_c F} \ln \frac{i}{i_0}$. For a fuel cell operating with a transfer coefficient of 0.45 activation losses versus current density are shown in Fig.7.

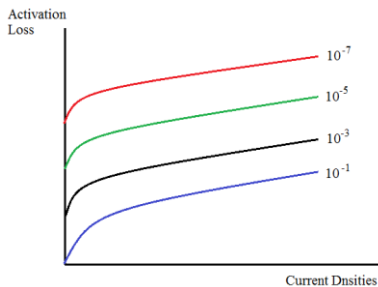


Figure 7. Activation loss as a function of current densities.

With an exchange current density of 10⁻³Acm⁻² activation losses for different transfer coefficients are shown in (Fig.8) which indicates that for large exchange current densities, fuel cell has insignificant activation over potential. This is a measure of the system abilities for delivering a net current with significant energies loss. When the transfer's coefficients are low,

the activation over potentials is large for any specific current. If the transfer's coefficients are large, the fuel cell will provide a large current with small activation over potential. The electrolytes have an intrinsic resistance to prevent the charge flow due to ohmic polarization including $R_{electronic}$ and R_{ionic} . Fuel cell resistances can be written as: $V_{ohmic} = iR_{ohmic} = i(R_{electronic} + R_{ionic})$. R_{ionic} Indicates the ionic resistance and $R_{electronic}$ consist of the total electrical resistance of all components concluding bipolar plates, cell interconnects and all connection paths.

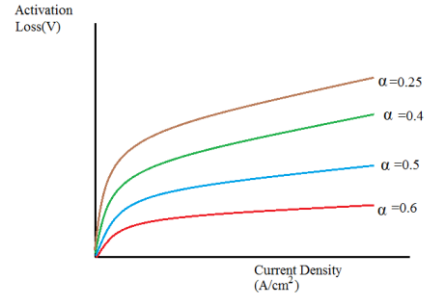


Figure 8. Activation loss versus transfer coefficient.

The big amount of ohmic loss appears during the transport of ions through the membrane which depends on membrane water or membrane relative humidity (ϕ_m) parameter as a function of $\lambda = C_0 + C_1\phi_m + C_2\phi_m^2 + C_3\phi_m^3 + C_4\phi_m^4 + \dots$ where C_n are coefficients. It is notable that the resistance of the membrane changes with water because of water uptake results in membrane swelling, which changes the membrane thickness along with its conductivity. The ionic resistance can be written as: $R_{electronic} = \frac{2l_d}{\sigma_a}$ where l_d and σ_a are diffusion layers of thickness and electronic conductivities, respectively. The concentration over potential is due to the mass transfer of H₂ and O₂. When the PEMFC cathode (O₂) and the anode (H₂) gases interact as an electrochemical process, the concentration of the H₂ and O₂ at the two electrodes will be consumed, that is lower than the initial concentration, and the irreversible loss caused by this concentration gradient is called the concentration over potential. The concentration over potential can be expressed as $V_{conc} = C \ln\left(\frac{i_L}{i_L - i}\right)$. Where i_L indicates that the PEMFC can reach the limiting current density during operation and c indicates the concentration loss constant.

3.1. Ni-Based Cermet Anodes.

For SOFCs at temperature 800 °C, the electrochemical polarization resistances for fuel oxidation in the anode is usually less compares to the electrochemical polarization resistances for O₂ reduction cathode electrode. Obviously, as the temperature is decreased to under 650 °C, the electrochemical polarization resistances in the anode is going to more dominant than that at the cathode. As exhibited in equation (1 &2), increasing the TPB length can effectively decrease the electrochemical polarization resistance of the anode. Fabricating nanomaterials in anode is not an easy way due to metal catalysts such as Ni. Metal-phase agglomeration leads to irreversible cell efficiency. The designing of the nanomaterials layer were aimed to suppress the agglomeration of Ni and to support less than 1 µm-thick electrolyte. High anode efficiency at low temperature might be achieved by introducing an anode functional layer (AFL). The

interfacial resistance of the anode supported SOFCs usually become more dominant at intermediate temperature rezone [87-90]. When the AFL thicknesses were decreased from 13.0 to 10.0 μm , the concentration polarization decreased. Hyun's group [91] a few years ago investigated NiO-YSZ nanocomposite materials for AFL that displayed high performances in Ni-YSZ-based cells. Lee et al. exhibited that the nanocomposite Ni-Gd_{0.1}Ce_{0.9}

O_{1.95} AFL deposited on the anode supports by dip coating process had better Ni and Ce distribution. The AFL thicknesses were about 23-24 μm . In addition, the interface among the electrolytes and the AFL seems to be well-connected. Gao and coworkers illustrated that SOFCs produced via a new processing technique and a La_{0.2}Sr_{0.8}TiO_{3- δ} (LST) shown high power densities [92-96].

4. CONCLUSIONS

Hydrogen fuel cells will play a significant role in the transportation industry in the near future. The price of fuel cells will reduce in producing fuel cells in large quantities and commercializing them. Modelling and controlling of ion transport rate efficiency can be investigated for various fuel cells in viewpoint of voltage output data. Controlling T, P, d_{mem} , and the water contents (λ) of the proton exchange membranes between the ideal state and the saturated state at any time can strongly improve the optimal output power densities of an irreversible PEMFC, AFC, DMFC, PAFC, DFAFC, and DCFC fuel cells.

Also mixing of fuel cells with the novel Nanotechnologies such as lithium ion batteries can be useful as interdisciplinary sciences. This recent development exhibit the situation and quality of basic research need to continue unabated. Tight efforts have been done to develop LT-SOFCs that can operate between 550 and 680 °C. By reducing the temperature further to between 350 and 550 °C, the application of SOFCs can be extended to transportation, military, and portable needs. Low-cost compressive gasket seals can be used in this temperature range.

5. REFERENCES

- Schmidt-Rohr, K. How Batteries Store and Release Energy: Explaining Basic Electro chemistry. *J. Chem. Educ.* **2018**, *95*, 1801-1810, <https://doi.org/10.1021/acs.jchemed.8b00479>.
- Ciureanu, M. Effects of nafion dehydration in pem fuel cells. *Journal of Applied Electrochemistry* **2004**, *34*, 705-714, <https://doi.org/10.1023/B:JACH.0000031102.32521.c6>.
- Cruz-Manzo, S.; Chen, R.; Rama, P. Study of current distribution and oxygen diffusion in the fuel cell cathode catalyst layer through electrochemical impedance spectroscopy. *International Journal of Hydrogen Energy* **2013**, *38*, 1702-1713, <https://doi.org/10.1016/j.ijhydene.2012.08.141>.
- de Bruijn, F.A.; Dam, V.A.T.; Janssen, G.J.M. Review: Durability and degradation issues of PEM fuel cell components. *Fuel Cells* **2008**, *8*, 22, <https://doi.org/10.1002/fuce.200700053>.
- Wang, J.Y. Pressure drop and flow distribution in parallel-channel of configurations of fuel cell stacks: U-type arrangement. *International Journal of Hydrogen Energy* **2008**, *33*, 6339-6350, <https://doi.org/10.1016/j.ijhydene.2008.08.020>.
- Dohle, H.; Mergel, J.; Stolten, D. Heat and power management of a direct-methanol-fuel-cell (DMFC) system. *Journal of Power Sources* **2002**, *111*, 268-282, [https://doi.org/10.1016/S0378-7753\(02\)00339-7](https://doi.org/10.1016/S0378-7753(02)00339-7).
- Wei, Y.; Almheiri, S.; Shen, L.L.; Zhang, X.; Guo, Z.; Zhu, H.; Liu, H. A novel membrane for DMFC - Na₂Ti₃O₇ Nanotubes/Nafion @ composite membrane: Performances studies. *International Journal of Hydrogen Energy* **2012**, *37*, 1857-1864, <https://doi.org/10.1016/j.ijhydene.2011.08.107>.
- Saif, M.; Liu, H. Effect of cathode catalyst layer thickness on methanol cross-over in a DMFC. *Electrochimica Acta* **2010**, *56*, 600-606, <https://doi.org/10.1016/j.electacta.2010.09.001>.
- Saif, A.; Liu, H. Separate measurement of current density under land and channel in Direct Methanol Fuel Cells. *Journal of Power Sources* **2014**, *246*, 899-905, <https://doi.org/10.1016/j.jpowsour.2013.08.029>.
- Motoo, S.; Watanabe, M. Electrolysis by Ad-Atoms Part II. Enhancement of the Oxidation of Methanol on Platinum by Ruthenium Ad-Atoms. *Electrochemistry and Interfacial Electrochemistry* **1975**, *60*, 267-273, [https://doi.org/10.1016/S0022-0728\(75\)80261-0](https://doi.org/10.1016/S0022-0728(75)80261-0).
- Ha, S.; Larsen, R.; Masel, R.I. Performance characterization of Pd /C Nano-catalyst for direct formic acid fuel cells. *Journal of Power Sources* **2005**, *144*, 28-34, <https://doi.org/10.1016/j.jpowsour.2004.12.031>.
- Monajjemi, M.; Honaparvar, B.; Hadad, B.K.; Ilkhani, A.R.; Mollaamin F. Thermo-chemical investigation and NBO analysis of some anxiotoxic as Nano- drugs. *African journal of pharmacy and pharmacology* **2010**, *4*, 521-529.
- Adler, S.B.; Lane, J.A.; Steele, B.C.H. Electrode kinetics on porous mixed - conducting oxygen electrodes, *J. Electrochem. Soc.* **1996**, *143*, 3554. <https://doi.org/10.1149/1.1837252>.
- Lu, Y.; Kreller, C.; Adler, S.B. Solid gas electrochemical interface, *J. Electrochem. Soc.* **2009**, *156*, B513.
- Monajjemi, M.; Afsharnezahed, S.; Jaffari, M.R.; Mirdamadi, S.; Mollaamin, F.; Monajemi, H.; Investigation of energy and NMR isotropic shift on the internal rotation Barrier of Θ_4 dihedral angle of the DLPC: A GIAO study, *Chemistry*, **2008**, *17*(1), 55-69.
- Laguna-Bercero, M.A.; Campana, R.; Larrea, A.; Kilner, J.A.; Orera, V.M. Performance and Aging of Microtubular YSZ-based Solid Oxide Regenerative Fuel Cells. *Fuel Cells* **2011**, *11*, 116-123, <https://doi.org/10.1002/fuce.201000069>.
- Dönitz, W.; Erdle, E. High-temperature electrolysis of water vapor—status of development and perspectives for application. *International Journal of Hydrogen Energy* **1985**, *10*, 291-295, [https://doi.org/10.1016/0360-3199\(85\)90181-8](https://doi.org/10.1016/0360-3199(85)90181-8).
- Zhu, B.; Ingvar, A.; Andersson, C.; Borsand, K.; Nilsson, M.; Bengt-Erik, M. Electrolysis studies based on ceria-based composites. *Electrochemistry Communications* **2006**, *8*, 495-498, <https://doi.org/10.1016/j.elecom.2006.01.011>.
- Laguna-Bercero, M.A.; Skinnera; S.J.; Kilner, J.A. Performance of solid oxide electrolysis cells based on scandia stabilised zirconia. *Journal of Power Sources*. **2009**, *192*, 126-131, <https://doi.org/10.1016/j.jpowsour.2008.12.139>.
- Marina, O.A.; Pederson, L.R.; Williams, M.C.; Coffey, G.W.; Meinhardt, K.D.; Nguyen, C.D.; Thomsen, E.C. Electrode Performance in Reversible Solid Oxide Fuel Cells. *Journal of the Electrochemical Society* **2007**, *154*, B452, <https://doi.org/10.1149/1.2710209>.
- Laguna-Bercero, M.A.; Kilner; J.A.; Skinner, S.J. Development of oxygen electrodes for reversible solid oxide fuel cells with scandia stabilized zirconia electrolytes.

- Solid State Ionics* **2011**, *192*, 501–504, <https://doi.org/10.1016/j.ssi.2010.01.003>.
22. Hauch, A.; Jensen, S.H.; Ramousse, S.; Mogensen, M. Performance and Durability of Solid Oxide Electrolysis Cells. *Journal of the Electrochemical Society*. **2006**, *153*, A1741, <https://doi.org/10.1149/1.2216562>.
23. Monajjemi, M.; Noei, M.; Mollaamin, F.; Design of fMet-tRNA and calculation of its bonding properties by quantum mechanics, *Nucleosides, Nucleotides and Nucleic Acids*, 2010, *29*(9), 676–683, <https://doi.org/10.1080/15257771003781642>.
24. Badwal, S.P.S.; Giddey, S.; Kulkarni, A.; Goel, J.; Basu, S. Direct ethanol fuel cells for transport and stationary applications A comprehensive review. *Applied Energy*. **2015**, *145*, 80–103, <https://doi.org/10.1016/j.apenergy.2015.02.002>.
25. Badwal, S.P.S. Review of Progress in High Temperature Solid Oxide Fuel Cells. *Journal of the Australian Ceramics Society* **2014**, *50*, <https://doi.org/10.1002/chin.201531316>.
26. Badwal, S.P.S. Review of Progress in High Temperature Solid Oxide Fuel Cells. *Journal of the Australian Ceramics Society* **2015**, *50*, <https://doi.org/10.1002/chin.201531316>.
27. Minh, N.Q. ceramic fuel cells, *J. Am. Ceram. Soc.* **1993**, *76*, 563 <https://doi.org/10.1111/j.1151-2916.1993.tb03645.x>.
28. Monajjemi, M.; Ghiasi, R.; Abedi, A.; Theoretical investigation of the interaction of cytosine and its tautomers with alkali metals, *Russian Journal of Inorganic Chemistry*. **2005**, *50*(3), 282–388.
29. Jiang, N.; Wachsmann, E.D.; Jung, S.H. A higher conductivity Bi₂Os-based electrolyte, *Solid State Ionics*, **2002**, *150*, 347.
30. Monajjemi, M.; Ghiasi, R.; Theoretical study of borthiin and its derivatives: Structure and aromaticity. *Journal of Sulfur chemistry*, **2007**, 505–51128.
31. Takahashi, T.; Esaka, T.; Iwahara, H. *J. Appl. Electrochem.* **1975**, *5*, 197.
32. Jung, D.W.; Duncan, K.L.; Camaratta, M.A.; Kang, T.L.; Nino, J.C.; Wachsmann, E.D. *J. Am. Ceram. Soc.* **2010**, *93*, 1384.
33. Singh, P.; Goodenough, J.B. Monoclinic Sr_{1-x}N_xaxSiO_{3-0.5x}: new superior oxide ion electrolytes, *J. Am. Chem. Soc.* **2013**, *135*, 10149. <https://doi.org/10.1021/ja4042737>.
34. Kannan, R.; Singh, K.; Gill, S.; Fürstenthaupt, T.; Thangadurai, V.; chemically stable proton conducting doped BaCeO₃- No more fear to SOFC wastes, *Sci.Rep.* **2013**, *3*, 2138. <https://doi.org/10.1038/srep02138>.
35. Yang, L.; Wang, S.; Blinn, K.; Liu, M.; Liu, Z.; Cheng, Z.; Liu, M. Enhanced sulfur and coking tolerance of a mixed ion conductor for SOFCs <https://doi.org/10.1126/science.1174811>.
36. Liu, Y.; Zha, S.; Liu, M. Novel Nanostructured electrodes for solid oxide fuel cells fabricated by combustion chemical vapour deposition, *Adv. Mater.* **2004**, *16*, 256. <https://doi.org/10.1002/adma.200305767>.
37. Monajjemi, M.; Ahmadianarog, N.T. S-NICS: An aromaticity criterion for nano molecules, *Journal of Computational and Theoretical Nanoscience*, **2015**, *12*(11), 4895–4914.
38. Monajjemi, M.; Farahani, N.; Mollaamin, F.; Thermodynamic study of solvent effects on nanostructures: Phosphatidylserine and phosphatidylinositol membranes, *Physics and Chemistry of Liquids*, 2012, *50*(2), 161–172 <https://doi.org/10.1080/00319104.2010.527842>.
39. Rowe, A.; Li, X. Mathematical modeling of proton exchange membrane fuel cells. *Journal of Power Sources* **2001**, *102*, 82–96, [https://doi.org/10.1016/S0378-7753\(01\)00798-4](https://doi.org/10.1016/S0378-7753(01)00798-4).
40. Siegel, C. Review of computational heat and mass transfer modeling in polymer electrolyte-membrane (pem) fuel cells. *Energy* **2008**, *33*, 1331–1352, <https://doi.org/10.1016/j.energy.2008.04.015>.
41. Yao, K.Z.; Karan, K.; McAuley, K.B.; Oosthuizen, P.; Peppley, B.; Xie, T. A review of mathematical models for hydrogen and direct methanol polymer electrolyte membrane fuel cells. *Fuel Cells* **2004**, *4*, 3–29, <https://doi.org/10.1002/fuce.200300004>.
42. Pukrushpan, J.T.; Peng, H.; Stefanopoulou, A.G. Control-oriented modeling and analysis for automotive fuel cell systems. *Journal of Dynamic Systems, Measurement, and Control* **2004**, *126*, *14*, [https://doi.org/10.1016/S1474-6670\(17\)30386-5](https://doi.org/10.1016/S1474-6670(17)30386-5).
43. Tao, W.Q.; Min, C.H.; Liu, X.L.; He, L.Y.; Yin, B.H.; Jiang, W. Parameter sensitivity examination and discussion of PEM fuel cell simulation model validation: Part i. current status of modeling research and model development. *Journal of Power Sources* **2006**, *160*, 359–373, <https://doi.org/10.1016/j.jpowsour.2006.01.078>.
44. Karimi, G. Along-channel flooding prediction of polymer electrolyte membrane fuel cells. *International Journal of Energy Research* **2011**, *35*, 883–896, <https://doi.org/10.1002/er.1746>.
45. Eriksson, E.L.V.; Gray, E.M.A. Optimization and integration of hybrid renewable energy hydrogen fuel cell energy systems— A critical review. *Appl. Energy* **2017**, *202*, 348–364, <https://doi.org/10.1016/j.apenergy.2017.03.132>.
46. Costilla-Reyes, A.; Erbay, C.; Carreon-Bautista, S.; Han, A.; Sánchez-Sinencio, E. A Time-Interleave-Based Power Management System with Maximum Power Extraction and Health Protection Algorithm for Multiple Microbial Fuel Cells for Internet of Things Smart Nodes. *Appl. Sci.* **2018**, *8*, 2404, <https://doi.org/10.3390/app8122404>.
47. Kerviel, A.; Pesyridis, A.; Mohammed, A.; Chalet, D.; Kerviel, A.; Pesyridis, A.; Mohammed, A.; Chalet, D. An Evaluation of Turbocharging and Supercharging Options for High-Efficiency Fuel Cell Electric Vehicles. *Appl. Sci.* **2018**, *8*, 2474, <https://doi.org/10.3390/app8122474>.
48. Somekawa, T.; Nakamura, K.; Kushi, T.; Kume, T.; Fujita, K.; Yakabe, H. Examination of a high-efficiency solid oxide fuel cell system that reuses exhaust gas. *Appl. Therm. Eng.* **2017**, *114*, 1387–1392, <https://doi.org/10.1016/j.applthermaleng.2016.10.096>.
49. Chakraborty, U.K. A New Model for Constant Fuel Utilization and Constant Fuel Flow in Fuel Cells. *Appl. Sci.* **2019**, *9*, 1066, <https://doi.org/10.3390/app9061066>.
50. Choi, H.; Shin, J.; Woo, J. Effect of electricity generation mix on battery electric vehicle adoption and its environmental impact. *Energy Policy* **2018**, *121*, 13–24, <https://doi.org/10.1016/j.enpol.2018.06.013>.
51. Boretti, A. Novel dual fuel diesel-ammonia combustion system in advanced TDI engines. *Int. J. Hydrogen Energy* **2017**, *42*, 7071–7076, <https://doi.org/10.1016/j.ijhydene.2016.11.208>.
52. Hibino, T.; Kobayashi, K.; Nagao, M.; Teranishi, S. Hydrogen Production by Direct Lignin Electrolysis at Intermediate Temperatures. *ChemElectroChem* **2017**, *4*, 3032–3036, <https://doi.org/10.1002/celec.201700917>.
53. Hori, T.; Ma, Q.; Kobayashi, K.; Nagao, M. Electrolysis of humidified methane to hydrogen and carbon dioxide at low temperatures and voltages. *Int. J. Hydrogen Energy* **2019**, *44*, 2454–2460, <https://doi.org/10.1016/j.ijhydene.2018.12.044>.
54. Yang, G.; Jung, W.; Ahn, S.J.; Lee, D.; Yang, G.; Jung, W.; Ahn, S.J.; Lee, D. Controlling the Oxygen Electrocatalysis on Perovskite and Layered Oxide Thin Films for Solid Oxide Fuel Cell Cathodes. *Appl. Sci.* **2019**, *9*, 1030, <https://doi.org/10.3390/app9051030>.
55. Wilberforce, T.; El-Hassan, Z.; Khatib, F.N.; Al Makky, A.; Baroutaji, A.; Carton, J.G.; Olabi, A.G. Developments of electric cars and fuel cell hydrogen electric cars. *Int. J. Hydrogen Energy* **2017**, *42*, 25695–25734, <https://doi.org/10.1016/j.ijhydene.2017.07.054>.

56. Mollaamin, F. Monajjemi, M. DFT outlook of solvent effect on function of nano bioorganic drugs. *Physics and Chemistry of Liquids* **2012**, *50*, 596-604, <https://doi.org/10.1080/00319104.2011.646444>.
57. Mollaamin, F.; Gharibe, S.; Monajjemi, M. Synthesis of various nano and micro ZnSe morphologies by using hydrothermal method. *International Journal of Physical Sciences* **2011**, *6*, 1496-1500.
58. Ardalan, T.; Ardalan, P.; Monajjemi, M. Nano theoretical study of a C 16 cluster as a novel material for vitamin C carrier. *Fullerenes Nanotubes and Carbon Nanostructures* **2014**, *22*, 687-708, <https://doi.org/10.1080/1536383X.2012.717561>.
59. Mahdavian, L.; Monajjemi, M.; Mangkorntong, N. Sensor response to alcohol and chemical mechanism of carbon nanotube gas sensors. *Fullerenes Nanotubes and Carbon Nanostructures* **2009**, *17*, 484-495, <https://doi.org/10.1080/15363830903130044>.
60. Monajjemi, M.; Najafpour, J. Charge density discrepancy between NBO and QTAIM in single-wall armchair carbon nanotubes. *Fullerenes Nanotubes and Carbon Nano structures* **2014**, *22*, 575-594, <https://doi.org/10.1080/1536383X.2012.702161>.
61. Monajjemi, M.; Hosseini, M.S. Non bonded interaction of B16 N16 nano ring with copper cations in point of crystal fields. *Journal of Computational and Theoretical Nanoscience* **2013**, *10*, 2473-2477.
62. Monajjemi, M.; Mahdavian, L.; Mollaamin, F. Characterization of nanocrystalline silicon germanium film and nanotube in adsorption gas by Monte Carlo and Langevin dynamic simulation. *Bulletin of the Chemical Society of Ethiopia* **2008**, *22*, 277-286, <http://dx.doi.org/10.4314/bcse.v22i2.61299>.
63. Lee, V.S.; Nimmanpipug, P.; Mollaamin, F.; Thanasanvorakun, S.; Monajjemi, M. Investigation of single wall carbon nanotubes electrical properties and normal mode analysis: Dielectric effects. *Russian Journal of Physical Chemistry A* **2009**, *83*, 2288-2296, <https://doi.org/10.1134/S0036024409130184>.
64. Mollaamin, F.; Najafpour, J.; Ghadami, S.; Akrami, M.S.; Monajjemi, M. The electromagnetic feature of B N H (x = 0, 4, 8, 12, 16, and 20) nano rings: Quantum theory of atoms in molecules/NMR approach. *Journal of Computational and Theoretical Nanoscience* **2014**, *11*, 1290-1298.
65. Monajjemi, M.; Mahdavian, L.; Mollaamin, F.; Honarparvar, B. Thermodynamic investigation of enolketo tautomerism for alcohol sensors based on carbon nanotubes as chemical sensors. *Fullerenes Nanotubes and Carbon Nanostructures* **2010**, *18*, 45-55, <https://doi.org/10.1080/15363830903291564>.
66. Monajjemi, M.; Ghiasi, R.; Seyed Sadjadi, M.A. Metal-stabilized rare tautomers: N4 metalated cytosine (M = Li, Na, K, Rb and Cs), theoretical views. *Applied Organometallic Chemistry* **2003**, *17*, 635-640, <https://doi.org/10.1002/aoc.469>.
67. Ilkhani, A.R.; Monajjemi, M. The pseudo Jahn-Teller effect of puckering in pentatomic unsaturated rings C A E, A=N, P, As, E= H, F, Cl. *Computational and Theoretical Chemistry* **2015**, *1074*, 19-25.
68. Monajjemi, M. Non-covalent attraction of B N and repulsion of B N in the B N ring: a quantum rotatory due to an external field. *Theoretical Chemistry Accounts* **2015**, *134*, 1-22, <https://doi.org/10.1007/s00214-015-1668-9>.
69. Monajjemi, M.; Naderi, F.; Mollaamin, F.; Khaleghian, M. Drug design outlook by calculation of second virial coefficient as a nano study. *Journal of the Mexican Chemical Society* **2012**, *56*, 207-211, <https://doi.org/10.29356/jmcs.v56i2.323>.
70. Monajjemi, M.; Bagheri, S.; Moosavi, M.S. Symmetry breaking of B2N(-,0,+): An aspect of the electric potential and atomic charges. *Molecules* **2015**, *20*, 21636-21657, <https://doi.org/10.3390/molecules201219769>.
71. Monajjemi, M.; Mohammadian, N.T. S-NICS: An aromaticity criterion for nano molecules. *Journal of Computational and Theoretical Nanoscience* **2015**, *12*, 4895-4914, <https://doi.org/10.1166/jctn.2015.4458>.
72. Monajjemi, M.; Ketabi, S.; Hashemian Zadeh, M.; Amiri, A. Simulation of DNA bases in water: Comparison of the Monte Carlo algorithm with molecular mechanics force fields. *Biochemistry (Moscow)* **2006**, *71*, 1-8, <https://doi.org/10.1134/s0006297906130013>.
73. Monajjemi, M.; Lee, V.S.; Khaleghian, M.; Honarparvar, B.; Mollaamin, F. Theoretical Description of Electromagnetic Nonbonded Interactions of Radical, Cationic, and Anionic NH2BHNBNH2 Inside of the B18N18 Nanoring. *J. Phys. Chem C* **2010**, *114*, 15315, <http://dx.doi.org/10.1021/jp104274z>.
74. Monajjemi, M.; Boggs, J.E. A New Generation of BnNn Rings as a Supplement to Boron Nitride Tubes and Cages. *J. Phys. Chem. A* **2013**, *117*, 1670-1684, <http://dx.doi.org/10.1021/jp312073q>.
75. Monajjemi, M. Non bonded interaction between BnNn (stator) and BN B (rotor) systems: A quantum rotation in IR region. *Chemical Physics* **2013**, *425*, 29-45, <https://doi.org/10.1016/j.chemphys.2013.07.014>.
76. Monajjemi, M.; Robert, W.J.; Boggs, J.E. NMR contour maps as a new parameter of carboxyl's OH groups in amino acids recognition: A reason of tRNA-amino acid conjugation. *Chemical Physics* **2014**, *433*, 1-11, <https://doi.org/10.1016/j.chemphys.2014.01.017>.
77. Monajjemi, M. Quantum investigation of non-bonded interaction between the B15N15 ring and BH2NBH2 (radical, cation, and anion) systems: a nano molecular motor. *Struct Chem* **2012**, *23*, 551-580, <http://dx.doi.org/10.1007/s11224-011-9895>.
78. Monajjemi, M. Metal-doped graphene layers composed with boron nitride-graphene as an insulator: a nano-capacitor. *Journal of Molecular Modeling* **2014**, *20*, 2507, <https://doi.org/10.1007/s00894-014-2507-y>.
79. Monajjemi M. Graphene/(h-BN)*n*/X-doped raphene as anode material in lithium ion batteries (X = Li, Be, B AND N). *Macedonian Journal of Chemistry and Chemical Engineering* **2017**, *36*, 101-118, <http://dx.doi.org/10.20450/mjccc.2017.1134>.
80. Monajjemi, M.; Dang, C. M.; Alihosseini, A.; Mollaamin, F. Designing BN sheets of X-G/(h-BN)*n*/X-G (X = B, N) and GO/h-BN/GO structures for based anodes material to improve the performance of lithium-ion batteries. *Int. J. Nanotechnology* **2018**, *15*, 819-844, <https://doi.org/10.1504/IJNT.2018.099925>.
81. Phm, T.T.; Monajjemi, M.; Dang, C.M. Fabrication of lithium-ion batteries based on various LiNi1-xCoxO2 cathode materials. *Int. J. Nanotechnol.* **2018**, *15*, 925-935, <https://doi.org/10.1504/IJNT.2018.099932>.
82. Thi L.C.M.; Blanc, E.F.; Monajjemi, M.; Dang, C.M. Theoretical and experimental simulation of inkjet printing process: investigation of physical parameters of a droplet. *Int. J. Nanotechnol.*, **2018**, *15*, 11, 845-857, <https://doi.org/10.1504/IJNT.2018.099926>.
83. Monajjemi, M. Cell membrane causes the lipid bilayers to behave as variable capacitors: A resonance with self-induction of helical proteins. *Biophysical Chemistry* **2015**, *207*, 114-127, <https://doi.org/10.1016/j.bpc.2015.10.003>.
84. Monajjemi, M. Study of CD5+ Ions and Deuterated Variants (CHxD(5-x)+): An Artefactual Rotation. *Russian Journal of Physical Chemistry a* **2018**, *92*, 2215-2226, <https://doi.org/10.1134/S0036024418110286>.
85. Monajjemi, M. Study of CD5+ Ions and Deuterated Variants (CHxD(5-x)+): An Artefactual Rotation. *Russian Journal of*

Physical Chemistry a **2018**, *92*, 2215–2226, <https://doi.org/10.1134/S0036024418110286>.

86. Monajjemi, M. Liquid-phase exfoliation (LPE) of graphite towards graphene: An ab initio study. *Journal of Molecular Liquids* **2017**, *230*, 461–472, <https://doi.org/10.1016/j.molliq.2017.01.044>.

87. Jalilian, H.; Monajjemi, M. Capacitor simulation including of X-doped graphene (X = Li, Be, B) as two electrodes and BN_m (m = 1–4) as the insulator. *Japanese Journal Applied Physics* **2015**, *54*, 085101–7.

88. Bhosale, A.C.; Mane, S.R.; Singdeo, D.; Ghosh, P.C. Modeling and experimental validation of a unitized regenerative fuel cell in electrolysis mode of operation. *Energy* **2017**, *121*, 256–263, <https://doi.org/10.1016/j.energy.2017.01.031>.

89. Ito, H.; Miyazaki, N.; Ishida, M.; Nakano, A. Efficiency of unitized reversible fuel cell systems. *Int. J. Hydrogen Energy* **2016**, *41*, 5803–5815, <https://doi.org/10.1016/j.ijhydene.2016.01.150>.

90. Hardman, S.; Tal, G. Who are the early adopters of fuel cell vehicles? *Int. J. Hydrogen Energy* **2018**, *43*, 17857–17866, <https://doi.org/10.1016/j.ijhydene.2018.08.006>.

91. Robledo, C.B.; Oldenbroek, V.; Abbruzzese, F.; van Wijk, A.J.M. Integrating a hydrogen fuel cell electric vehicle with

vehicle-to-grid technology, photovoltaic power and a residential building. *Appl. Energy* **2018**, *215*, 615–629, <https://doi.org/10.1016/j.apenergy.2018.02.038>.

92. Lee, J.J.; Moon, H.; Park, H.G.; Yoon, D.I.; Hyun, S.H. Applications of nano-composite materials for improving the performance of anode-supported electrolytes of SOFCs *Int. J. Hydrogen Energy* **2010**, *35*, 738.

93. Brey, J.J.; Carazo, A.F.; Brey, R. Exploring the marketability of fuel cell electric vehicles in terms of infrastructure and hydrogen costs in Spain. *Renew. Sustain. Energy Rev.* **2018**, *82*, 2893–2899, <https://doi.org/10.1016/j.rser.2017.10.042>.

94. He, X.; Jiang, Y. Review of hybrid electric systems for construction machinery. *Autom. Constr.* **2018**, *92*, 286–296, <https://doi.org/10.1016/j.autcon.2018.04.005>.

95. Dreier, D.; Silveira, S.; Khatiwada, D.; Fonseca, K.V.O.; Nieweglowski, R.; Schepanski, R. Well-to-Wheel analysis of fossil energy use and greenhouse gas emissions for conventional, hybrid-electric and plug-in hybrid-electric city buses in the BRT system in Curitiba, Brazil. *Transp. Res. Part D Transp. Environ.* **2018**, *58*, 122–138, <https://doi.org/10.1016/j.trd.2017.10.015>.

96. Bizon, N.; Thounthong, P. Fuel economy using the global optimization of the Fuel Cell Hybrid Power Systems. *Energy Convers. Manag.* **2018**, *173*, 665–678, <https://doi.org/10.1016/j.enconman.2018.08.015>.

6. ACKNOWLEDGEMENTS

This research is funded by Vietnam National University – Ho Chi Minh City (VNU-HCM) under the grant number TX2019-32-01.



© 2019 by the authors. This article is an open access article distributed under the terms and conditions of the Creative Commons Attribution (CC BY) license (<http://creativecommons.org/licenses/by/4.0/>).